Oxidation of the Mn Cluster Induces Structural Changes of NO_3^- Functionally Bound to the Cl^- Site in the Oxygen-Evolving Complex of Photosystem II

Koji Hasegawa, Yukihiro Kimura, and Taka-aki Ono
Laboratory for Photo-Biology (I), RIKEN Photodynamics Research Center, The Institute of Physical and Chemical Research, 519-1399 Aoba, Aramaki, Aoba, Sendai 980-0845, Japan

ABSTRACT Cl^- is an indispensable cofactor for photosynthetic O_2 evolution and is functionally replaced by NO_3^-. Structural changes of an isotopically labeled NO_3^- ion, induced by the oxidation of the Mn cluster (S_1-to-S_2), were detected by FTIR spectroscopy. NO_3^--substituted photosystem II core particles showed $^{14}N^{16}O_3^-/^{15}N^{16}O_3^-$ and $^{14}N^{16}O_3^-/^{14}N^{18}O_3^-$ isotopic bands in the S_2/S_1 spectra with markedly high signal/noise ratio. These bands appeared only in the region from 1415 to 1284 cm^{-1}, indicating that the bands do not arise from a metal-bound NO_3^- but from an ionic NO_3^-. The intensity of the bands exhibited a quantitatively proportional relationship with the O_2 activity. These results demonstrate that the NO_3^- functionally bound to the Cl^- site couples to the Mn cluster structurally, but is not associated with the cluster as a direct ligand. Comparison of the bands for two isotopes (^{15}N and ^{18}O) and their simulations enable us to assign each band to the S_1 and S_2 states. The results indicate that the NO_3^- ion bound to the Cl^- site is highly asymmetric in S_1 but rather symmetric in S_2. Since NO_3^- functionally replaces Cl^-, most of the conclusions drawn from this study will be also applicable to Cl^-.

INTRODUCTION

Photosynthetic water oxidation occurs in the OEC residing on the donor side of PS II, in which a tetranuclear Mn cluster catalyzes the oxidation of two water molecules to one oxygen molecule through the cycling of five intermediate states labeled S_0–S_4, where S_1 is thermally stable in the dark (reviewed in Debus, 1992; Goussias et al., 2002). Cl^- is known to be an indispensable inorganic cofactor for photosynthetic water oxidation, and O_2 evolution is completely inhibited in the absence of Cl^- and restored by replenishment of Cl^- (Crichley, 1985; Homann, 1987, 2002; Debus, 1992; Goussias et al., 2002; but see Olesen and Andréasson, 2003). Radioisotope labeling studies have suggested that PS II has a binding site for approximately one Cl^- ion per unit of PS II (Lindberg et al., 1990; Lindberg and Andréasson, 1996). In eukaryotes, 16- and 24-kDa extrinsic proteins function as concentrators for Cl^- and barriers to free diffusion of Cl^- between the site and aqueous solvent, and the depletion of these proteins therefore decreases the affinity of Cl^- for its binding site and induces rapid exchange of Cl^- (Akabori et al., 1984; Miyao and Murata, 1985; Homann, 1988; Lindberg et al., 1993). It has been shown the S state transition is interrupted after reaching the S_2 state (Itoh et al., 1984; Theg et al., 1984; Homann et al., 1986; Ono et al., 1986, 1995). UV absorption studies have revealed that Cl^- is required for the S_2-to-S_3 and S_3-to-S_0 transitions (Wincencjusz et al., 1997). EPR and thermoluminescence studies indicate that the magnetic and redox properties of the Mn cluster are modified in the absence of Cl^-. In addition, an FTIR study indicated that the structure of protein matrices including the putative ligands for the Mn cluster is distorted in the absence of Cl^- (Hasegawa et al., 2002). Apart from its functional roles, Cl^- is required for stable preservation of the Mn cluster. In the absence of the 33-kDa extrinsic protein, the Mn cluster is destroyed when Cl^- concentration in the medium is too low (Ono and Inoue, 1985). The significant influence of Cl^- depletion on both the functional and structural properties of the Mn cluster indicates that the Cl^- is in close proximity to the Mn cluster. The Mn x-ray absorption spectrum of PS II particles from cyanobacteria cultured in a medium supplemented with Br^- as a replacement for Cl^- reveals some change in the Fourier peak, which has been assumed to involve back scattering from Br^- (Klein et al., 1993). Nuclear coupling between the halide and the Mn cluster was suggested from electron spin-echo envelope modulation of the multiline EPR signal in some Br^--substituted membrane samples (Boussac, 1995). It has been widely proposed that Cl^- is directly associated with the Mn ions in the cluster as a direct ligand (Boussac, 1995; Casey and Sauer, 1984); however, no conclusive experimental evidence supporting this view has been obtained. Cl^- is functionally replaced by some other monovalent anions, of which, apart from the halides, NO_3^- is the most effective. The NO_3^--substituted OEC is fully active in O_2 evolution but has a slower turnover rate (Sinclair, 1994; Wincencjusz et al., 1998; Hasegawa et al., 2002), probably at the S_3-to-S_0 transition (Wincencjusz et al., 1999). Therefore, it is rational to consider that NO_3^- is bound to the Cl^- site in a manner that is identical or

Submitted July 11, 2003, and accepted for publication September 22, 2003.
Address reprint requests to Koji Hasegawa or Taka-aki Ono, Tel.: +81-22-228-2047; Fax: +81-22-228-2045; E-mail: kojihase@postman.riken.go.jp or takaaki@postman.riken.go.jp.

Abbreviations used: Chl, chlorophyll; DCMU, 3-(3,4-dichlorophenyl)-1, 1-dimethylurea; EPR, electron paramagnetic resonance; FTIR, Fourier transform infrared; MES, 2-morpholinoethanesulfonic acid; OEC, oxygen-evolving complex; PS, photosystem; Q_A, primary quinone acceptor of photosystem II; Q_B, secondary quinone acceptor of photosystem II.

0006-3495/04/02/1042/09 $2.00

quite similar to that of Cl^- in principle, although some changes in the properties of the Mn cluster are induced in the NO_3^--substituted OEC. Competition between NO_3^- and Cl^- has also been suggested in a site for the slowly exchanging Cl^- (Lindberg et al., 1993).

In a previous study, we used FTIR spectroscopy to study the Cl^- function in OEC using PS II membrane samples (Hasegawa et al., 2002). The light-induced FTIR difference spectrum enabled us to probe subtle conformation and/or configuration changes induced by Cl^- depletion in protein matrixes of the OEC, including the ligands of the Mn cluster. In that study, we used $^{15}NO_3^-$ as a specific probe and succeeded in detecting the isotopic bands in the S_2/S_1 FTIR difference spectra in NO_3^--substituted PS II membranes. We tentatively interpreted the isotopic bands as being due to NO_3^- bound to the functional Cl^- site in the OEC because the further addition of excess Cl^- suppressed the formation of the isotopic bands. Accordingly, it was presumed, based on their band positions, that NO_3^-, and thereby Cl^-, structurally couples to the Mn cluster but does not bind to the Mn cluster as a direct ligand. However, the disappearance of the $^{14}NO_3^-/^{15}NO_3^-$ isotopic band on addition of excess Cl^- did not provide any conclusive evidence for the origin of the bands, since Cl^- may compete with NO_3^- in any adventitious binding sites for anions present in PS II, and expel NO_3^-. Also, the quality of the spectrum was too low to allow any quantitative evaluation of the bands and judgment on the presence of other isotopic bands in the spectrum. Therefore, much ambiguity remained in the interpretation of the bands.

In this study, to address these unresolved issues, we measured the isotopic difference FTIR spectra of $^{14}N^{16}O_3^-/^{14}N^{18}O_3^-$ as well as $^{14}N^{16}O_3^-/^{15}N^{16}O_3^-$ in highly active PS II core particles isolated from spinach. The amplitude of the observed isotopic bands in the core particles was ~4–5 times larger than those in the PS II membranes, and the signal-to-noise ratio of the spectrum was markedly improved. These results clearly demonstrate that the isotopic bands arise from NO_3^- functionally bound to the unique Cl^- site in the OEC. Therefore, the observed isotopic bands must include direct structural information regarding NO_3^-, and thereby Cl^-, bound to the functional Cl^- site, ligands for Cl^-, and their changes upon the oxidation of the Mn cluster. All of this is indispensable for understanding the function of Cl^- in the oxygen evolution but difficult to determine with other techniques. We discuss the vibrational modes of NO_3^- bound to the Cl^- site in conjunction with the changes in interaction between NO_3^-, and thus Cl^-, and its ligands upon the S_1-to-S_2 transition.

EXPERIMENTAL PROCEDURES

Sample preparations

PS II core particles were prepared from PS II enriched thylakoid membranes that were isolated from market spinach (Berthold et al., 1981) with modification (Ono and Inoue, 1985). The following procedures were performed under complete darkness or in dim green light unless otherwise noted. The PS II membranes in a medium containing 400 mM sucrose, 20 mM NaCl and 20 mM MES/NaOH (pH 6.5) (medium A) were solubilized at 3.5 mg of Chl/ml with 0.04% (w/v) Triton X-100 and 2.45% (w/v) *n*-Heptyl-β-D-thioglucoside for 15 min at 0°C. The sample suspension was diluted with medium A in amounts that had been optimized for each batch (usually 3.0–3.5 hold dilution), and then incubated for 10 min after addition of $CaCl_2$ to a final concentration of 20 mM. The suspension was centrifuged at 39,000 $\times$ *g* for 40 min to precipitate light-harvesting complexes. The PS II core particles in the supernatant were precipitated by centrifuging at 39,000 $\times$ *g* for 10 min after the addition of half-volume of 20% (w/v) polyethyleneglycol 1000 solution, and resuspended in medium A after two washes with the same medium. The resulting core particles showed a Chl *a*/Chl *b* ratio of >20 and activity of 2.5–3.0 mmole of O_2/mg of Chl/h. For Cl^- depletion, the dark-adapted core particles were suspended in a medium containing 2 M NaCl, 400 mM sucrose, 20 mM MES/NaOH (pH 6.5) at 0.5 mg of Chl/ml. The suspension was then incubated at 0°C for 25 min in complete darkness to ensure the complete removal of the 16- and 24-kDa extrinsic proteins, which had been partly retained in the core particles. The salt-treated core particles were extensively washed (at least seven times) with a medium containing 400 mM sucrose and 40 mM MES/NaOH (pH 6.5) supplemented with $^1/_{10}$ volume of a medium containing 100 mM $Ca(OH)_2$ and 300 mM MES (pH 6.4) (medium B). The Cl^- concentration in medium B was found to be less than 30 μM using Chloride Test (Merck, Germany). All chemicals for medium B were from Sigma Ultra except for $Ca(OH)_2$ (99.9%, Wako Pure Chemical Industries, Japan). The resulting Cl^--depleted particles were suspended in medium B at 0.25 mg of Chl/ml supplemented with indicated concentrations of NaCl or $NaNO_3$, and then incubated on ice for 1 min. No detectable changes were observed in the FTIR spectrum after a prolonged incubation time. For FTIR, sample suspensions included 0.1 mM DCMU for measuring the $S_2Q_A^-/S_1Q_A$ difference spectrum and 0.1 mM DCMU and 5 mM NH_2OH for the Q_A^-/Q_A difference spectrum. NH_2OH was added as NH_2OH solution (50% stock, Wako Pure Chemical Industries, Japan) prepared just before use. The sample pellet after centrifugation for 15 min at 176,000 $\times$ *g* was sandwiched between a pair of BaF_2 plates. $Na^{15}NO_3$ (99.5% ^{15}N enrichment) and $NaN^{18}O_3$ (77.8% ^{18}O enrichment) were purchased from Shoko Tsusho (Japan).

Measurements

FTIR spectra were recorded on an IFS-66V/S spectrophotometer (Bruker, Germany) equipped with an MCT detector at a resolution of 4 cm^{-1} at 250 K as described in Hasegawa et al. (2002). Samples were illuminated with a CW light

(2 mW/cm^2) passing through a long-pass filter (>620 nm) at 250 K for 10 s. Three to five spectra for different samples were averaged for conventional S_2/S_1 FTIR difference spectra, whereas 12–14 spectra were averaged to improve signal-to-noise ratio for detecting isotopic bands. The S_2/S_1 FTIR difference spectrum was obtained by subtracting the Q_A^-/Q_A difference spectrum from the $S_2Q_A^-/S_1Q_A$ difference spectrum after normalizing both spectra with respect to the intensity of the carbonyl stretching band of Q_A^- at 1479 cm^{-1} (Berthomieu et al., 1990; Noguchi et al., 1992, 1995a; Hienerwadel et al., 1996; Onoda et al., 2000; Kimura and Ono, 2001; Kimura et al., 2002; Hasegawa et al., 2002; but see Razeghifard et al., 1999). O_2-evolving activity was measured at 25°C using a Clark-type O_2 electrode in medium B, supplemented with the indicated concentration of NaCl or $NaNO_3$. 1 mM $Na_3Fe(CN)_6$ and 0.25 mM 2,6-dichloro-*p*-benzoquinone were included as electron acceptors.

RESULTS

Fig. 1 shows the concentration dependences of Cl^- and NO_3^- on the restoration of O_2 evolution. Under both the saturating (*open symbols*) and limiting (*closed symbols*) light conditions, the O_2 evolution of the Cl^--depleted core particles was below the detectable limit in the Cl^--free medium (<30 μM Cl^-), but the activity was markedly restored by Cl^- addition (*circles*) with the same Cl^- dependency to reach 70%–80% activity of the untreated control core particles. The O_2 evolution was markedly restored by NO_3^- addition (*squares*). The maximally restored activity was less than 30% of that by Cl^- under the saturating light conditions but was over 80% of that restored by Cl^- under the limiting light conditions. The apparent *K*m values of Cl^- and NO_3^- for the restoration of O_2 evolution were found to be ~4 and 6 mM, respectively, under the saturating and the limiting light conditions. These results show that the OEC is reversibly inactivated in an all-or-none manner in the absence of Cl^-, and the NO_3^--substituted OEC is active in oxygen evolution but has a lower turnover rate in the core particles.

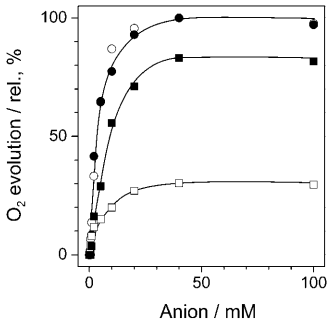

FIGURE 1 Dependence of O_2 evolution on Cl^- (*circles*) and NO_3^- (*squares*) concentration in Cl^--depleted PS II core particles under conditions of saturating light (*open symbols*) and limiting light (4% of the saturating light intensity) (*closed symbols*). 100% activity represents 2.1 and 0.37 mmole of O_2/mg of Chl/h for saturating and limiting light conditions, in which the O_2 evolution was assessed at 2.5 and 10 μg of Chl/ml, respectively.

Fig. 2 shows the effect of Cl^- depletion and NO_3^- substitution on the S_2/S_1 FTIR difference spectrum in the core particles. The S_2/S_1 spectrum was obtained by subtracting the Q_A^-/Q_A spectrum from the $S_2Q_A^-/S_1Q_A$ spectrum. The vibrational features of the S_2/S_1 spectrum (*spectrum a*, *solid curve*) in the untreated control core particles were almost the same as those in the PS II membranes, whereas the S/N ratio was approximately four times higher than that in the membranes. The Cl^- depletion (*spectrum b*) induced large changes in the amide modes and the carboxylate stretching modes for the putative carboxylate ligand(s) to the Mn cluster (Noguchi et al., 1995a,b; Noguchi and Sugiura, 2003). The replenishment of Cl^- restored a normal spectrum (*spectrum a*, *dotted curve*) that was almost indistinguishable from the untreated control spectrum. The amide bands at 1684(+), 1651(+), 1587(+), and 1547 (−) cm^{-1} and carboxylate bands at 1438(+)/1404(−) cm^{-1}, suppressed by the Cl^- depletion, were developed, whereas the bands prominent in the absence of Cl^- at 1695(+) and 1631(+) cm^{-1} diminished with increase in the NO_3^- concentration (*spectra c–g*). The dependence on the NO_3^- concentration of the intensity changes of the bands was roughly compatible with that of the recovery of O_2 evolution, although the band intensity was difficult to determine correctly due to overlapping of the bands. The overall features of the NO_3^--substituted FTIR difference spectrum (*spectrum g*) resembled those of the Cl^--reconstituted spectrum, but some differences were observed in the amide I mode at 1700–1600 cm^{-1} and bands at 1600–1500 cm^{-1}. Although the amide II and the asymmetric carboxylate modes overlapped in the latter region, the observed differences may be mainly ascribed to the change in the amide II mode in the NO_3^--substituted spectrum in accordance with

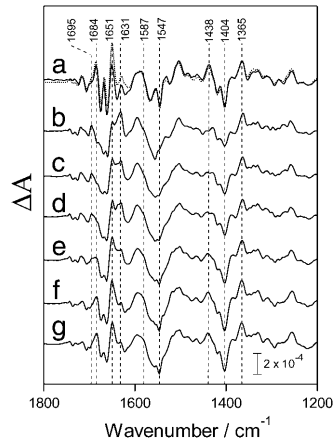

FIGURE 2 Light-induced S_2/S_1 FTIR difference spectra of untreated control PS II core particles (with 40 mM NaCl) (*a*, *solid line*), and Cl^--depleted core particles reconstituted with 40 mM NaCl (*a*, *dotted line*), and with 0 (Cl^--depletion) (*b*), 0.25 (*c*), 0.5 (*d*), 2 (*e*), 10 (*f*), and 40 mM (*g*) NO_3^-.

the change of the amide I mode. The amide modes are changed rather easily depending on the types of PS II preparations and by treatments of the samples even though they show the high O_2 activity. Therefore, it may be assumed that the binding of NO_3^- to the Cl^- site induces subtle formation changes in polypeptide backbone.

The functional replacement of Cl^- with NO_3^- indicates that NO_3^- is bound to the Cl^- site as a functional substitute for Cl^- in the core particles. Fig. 3 *A* shows the $^{14}N^{16}O_3^-$-substituted (*dotted curve*) and $^{15}N^{16}O_3^-$-substituted (*solid curve*) S_2/S_1 FTIR difference spectrum in the core particles. A distinct difference was observed in the region of 1420–1260 cm^{-1} between the two spectra. The quality of the obtained spectra was sufficiently high that it is clear that there is no observable difference between the two spectra except for the 1420–1260 cm^{-1} region as shown in the inset. Fig. 3 *B* shows the $^{14}N^{16}O_3^-$-substituted (*dotted curve*) and $^{14}N^{18}O_3^-$-substituted (*solid curve*) S_2/S_1 FTIR difference spectrum. The band shape of the $^{14}N^{18}O_3^-$-substituted spectrum in the region of 1420–1290 cm^{-1} clearly differed from the $^{14}N^{16}O_3^-$-substituted as well as the $^{15}N^{16}O_3^-$-substituted spectra. No difference was observed between the $^{14}N^{18}O_3^-$-substituted and $^{14}N^{16}O_3^-$-substituted spectra above 1420 and below 1280 cm^{-1}, as shown in the inset.

Fig. 4 shows the isotopic bands occurring in the NO_3^--substituted S_2/S_1 difference spectra in the core particles. Fig. 4 *A* shows the $^{14}N^{16}O_3^-/^{15}N^{16}O_3^-$ FTIR difference (*spectrum a*) and the $^{14}N^{16}O_3^-/^{14}N^{18}O_3^-$ difference (*spectrum b*) spectra for the $S_2Q_A^-/S_1Q_A$ difference, and the $^{14}N^{16}O_3^-/^{15}N^{16}O_3^-$ difference spectrum for the Q_A^-/Q_A difference (*spectrum c*). The $^{14}N^{16}O_3^-/^{15}N^{16}O_3^-$ (or $^{14}N^{16}O_3^-/^{14}N^{18}O_3^-$) difference spectrum for the $S_2Q_A^-/S_1Q_A$ difference was obtained by subtracting the $^{15}N^{16}O_3^-$ (or $^{14}N^{18}O_3^-$)-substituted $S_2Q_A^-/S_1Q_A$ spectrum from the $^{14}N^{16}O_3^-$-substituted $S_2Q_A^-/S_1Q_A$ spectrum. Since the Q_A^-/Q_A spectrum did not show any $^{14}N^{16}O_3^-/^{15}N^{16}O_3^-$ (*spectrum c*) and $^{14}N^{16}O_3^-/^{14}N^{18}O_3^-$ (data not shown) isotopic bands, instead of the S_2/S_1 spectra which were obtained by subtracting the Q_A^-/Q_A spectrum from the $S_2Q_A^-/S_1Q_A$ spectrum, we present the $S_2Q_A^-/S_1Q_A$ spectra due to the better signal quality. Hereafter, we use the $S_2Q_A^-/S_1Q_A$ difference spectrum for evaluating the isotopic bands for the S_2/S_1 difference, and denote these spectra simply as $^{14}N^{16}O_3^-/^{15}N^{16}O_3^-$ and $^{14}N^{16}O_3/^{14}N^{18}O_3^-$ spectra, unless otherwise noted. The $^{14}N^{16}O_3/^{15}N^{16}O_3^-$ spectrum (*spectrum a*) exhibited the distinct isotopic bands comprising major bands at 1369(+) and 1319(−) cm^{-1}, and minor bands at 1284(+) and 1415(−) cm^{-1}. The $^{14}N^{16}O_3^-/^{14}N^{18}O_3^-$ difference spectrum (*spectrum b*) exhibited pronounced isotopic bands in the 1420–1280 cm^{-1} region with similar band features to those in the $^{14}N^{16}O_3^-/^{15}N^{16}O_3^-$ spectrum. Except for these bands, no other isotopic band was found in the spectra over the frequency regions of 2140–940 cm^{-1}. It is particularly of note that the quality of the obtained spectra was remarkably high in comparison with that reported for PS II membranes (Hasegawa et al., 2002), in which the minor

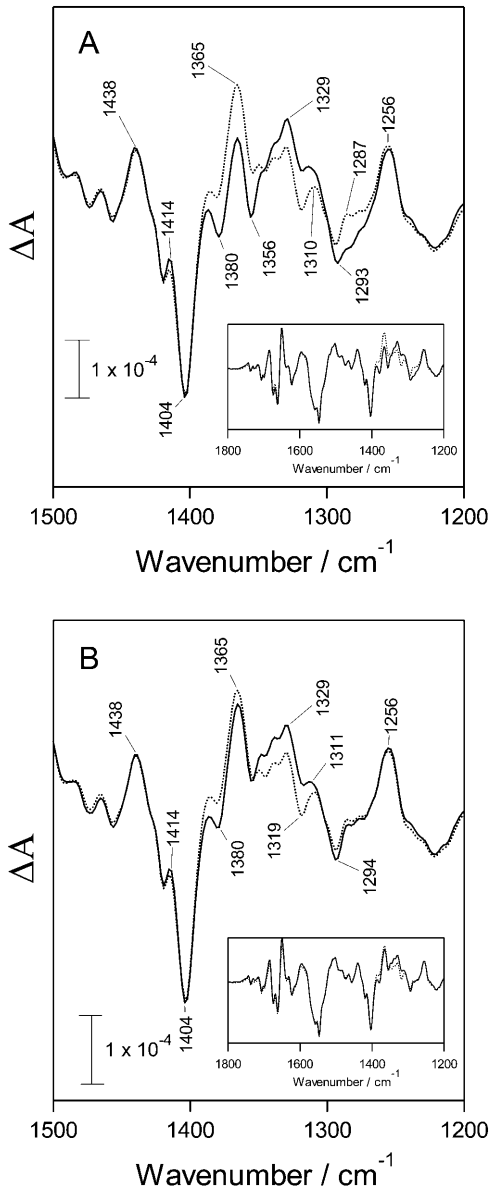

FIGURE 3 Light-induced S_2/S_1 FTIR difference spectra of Cl^--depleted PS II core particles that are reconstituted with 40 mM $Na^{14}N^{16}O_3$ (*A*, *B*: *dotted curve*), 40 mM $Na^{15}N^{16}O_3$ (*A*: *solid curve*), or 40 mM $Na^{14}N^{18}O_3$ (*B*: *solid curve*). The inset shows the light-induced S_2/S_1 FTIR difference spectra of the mid-IR region (1800–1200 cm^{-1}).

bands were concealed behind a high background noise level, which was even comparable to the intensity of the major bands in the 1700–1500 cm^{-1} region.

Fig. 4 *B* shows the expanded view of the $^{14}N^{16}O_3^-/^{15}N^{16}O_3^-$ (*solid curve*) and $^{14}N^{16}O_3^-/^{14}N^{18}O_3^-$ (*dotted curve*) spectra. The $^{14}N^{16}O_3^-/^{14}N^{18}O_3^-$ spectrum was presented after multiplying by a factor of 1.28 to account for the difference in ^{18}O enrichment (77.8%) compared with ^{15}N enrichment (99.5%) in $NaNO_3$. Two negative bands (denoted by *I* and *III*) and two positive bands (denoted by *II* and *IV*) were present in both difference spectra. However, the differences are distinct in the peak positions of the respective

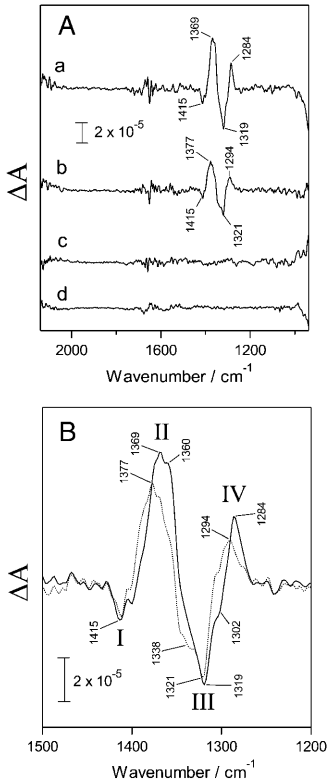

FIGURE 4 (*A*) $^{14}N^{16}O_3^-/^{15}N^{16}O_3^-$ (*a*) and $^{14}N^{16}O_3^-/^{14}N^{18}O_3^-$ (*b*) FTIR difference spectra for the $S_2Q_A^-/S_1Q_A$ difference, and $^{14}N^{16}O_3^-/^{15}N^{16}O_3^-$ FTIR difference spectra (*c*) for the Q_A^-/Q_A difference of mid-IR region (2140–940 cm^{-1}). The $^{14}N^{16}O_3^-/^{15}N^{16}O_3^-$ ($^{14}N^{16}O_3^-/^{14}N^{18}O_3^-$) spectrum was obtained by subtracting the $^{15}N^{16}O_3^-$ ($^{14}N^{18}O_3^-$) spectrum from the $^{14}N^{16}O_3^-$ spectrum. A dark-minus-dark FTIR spectrum (*d*) was presented to show the noise level. (*B*) Expanded view of the $^{14}N^{16}O_3^-/^{15}N^{16}O_3^-$ (*solid curve*) and $^{14}N^{16}O_3^-/^{14}N^{18}O_3^-$ (*dotted curve*) spectra for the $S_2Q_A^-/S_1Q_A$ difference in the region of 1500–1200 cm^{-1}. The $^{14}N^{16}O_3{}^-/^{14}N^{18}O_3^-$ spectrum was normalized by multiplication by a factor of 1.28 to compensate for the low ^{18}O (77.8%) enrichment in $NaNO_3$.

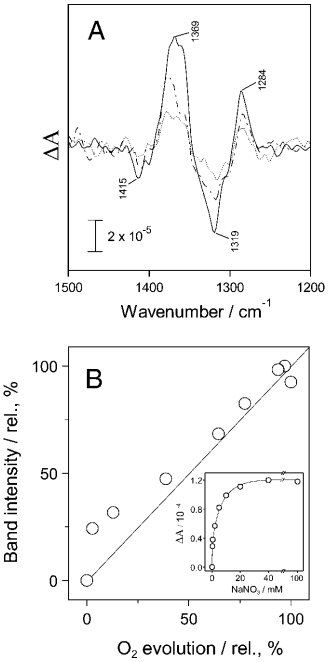

FIGURE 5 (*A*) $^{14}N^{16}O_3^-/^{15}N^{16}O_3^-$ FTIR difference spectrum for the $S_2Q_A^-/S_1Q_A$ difference in the presence of 0.25 mM (*dotted curve*), 2 mM (*hashed curve*), and 40 mM (*solid curve*) NO_3^-. The $^{14}N^{16}O_3^-/^{15}N^{16}O_3^-$ spectrum was obtained by subtracting the $^{15}N^{16}O_3^-$ ($S_2Q_A^-/S_1Q_A$) spectrum from the $^{14}N^{16}O_3^-$ ($S_2Q_A^-/S_1Q_A$) spectrum. (*B*) Relationship between the amplitude of the $^{14}N^{16}O_3^-/^{15}N^{16}O_3^-$ isotopic band and the restored O_2 evolution activity at various NO_3^- concentrations. The intensity of the isotopic band was estimated from the peak(1369 cm^{-1})-to-peak(1319 cm^{-1}) difference. The inset shows the dependence of the isotopic band intensity on NO_3^- concentration. The difference spectrum for the $S_2Q_A^-/S_1Q_A$ difference is identical to that for the S_2/S_1 difference but has a better signal/noise ratio.

bands, including the features of the shoulders at 1360, 1338, and 1302 cm^{-1}. These are apparently caused by the difference of the isotopic band shifts: an NO stretching band is downshifted by 31 cm^{-1} and 20 cm^{-1} in $^{15}N^{16}O_3^-$ and $^{14}N^{18}O_3^-$, respectively, as compared with naturally abundant $^{14}N^{16}O_3^-$ (Gatehouse et al., 1958). Band I, however, appeared similar in both isotopic difference spectra in terms of its intensity, shape, and position.

Fig. 5 shows the dependence of the amplitude of the $^{14}N^{16}O_3^-/^{15}N^{16}O_3^-$ isotopic bands on NO_3^- concentration. As shown in Fig. 5 *A*, the amplitude increased with the increase of the NO_3^- concentration, although the overall features of each spectrum were very similar. We therefore plotted the peak(1369 cm^{-1})-to-peak(1319 cm^{-1}) difference against the NO_3^- concentration as shown in the inset of Fig. 5 *B*. The band intensity reached the high saturation level at 40 mM NO_3^-, remaining constant up to 100 mM NO_3^-. The apparent *K*m value of NO_3^- for the isotopic band was found to be ~4 mM, which is comparable to that for the restoration of the O_2 evolution. In Fig. 5 *B*, the intensity of the $^{14}N^{16}O_3^-/^{15}N^{16}O_3^-$ isotopic bands was plotted against the restored O_2 evolution activity at various NO_3^- concentrations. The data points are mostly placed along the diagonal line including the origin of the coordinate axes, exhibiting a directly and quantitatively proportional relationship between the developed isotopic band and the restored O_2 evolution, except at the lower concentration of NO_3^-. This deviation may be mainly ascribed to the photoinactivation which may occur more severely in the Cl^--depleted than O_2-evolving OEC, and more efficiently during the activity assay at 25°C in the absence of DCMU than the FTIR measurements at 250 K in the presence of DCMU.

DISCUSSION

Origin of isotopic bands

In this study, we reported high quality isotopic spectra of NO_3^- for the S_2/S_1 difference using the PS II core particles, which enabled us to quantitatively evaluate the isotopic

bands. The intensity of $^{14}N^{16}O_3^-/^{15}N^{16}O_3^-$ isotopic bands exhibited a direct proportional relationship with the O_2 evolution restored by NO_3^- as shown in Fig. 5. Since the restored O_2 evolution activity by NO_3^- is proportional to the population of the active OECs that retain NO_3^- in their functional Cl^- site, the results clearly demonstrate that the isotopic bands do not arise from nonspecifically bound NO_3^- but from NO_3^- that is functionally bound to the Cl^- site and which structurally couples to the Mn cluster. The results also indicate that the structural changes of the NO_3^- and/or its protein ligand(s) responsible for the generation of the isotopic bands are closely correlated with the process of water oxidation. Since the NO_3^--substituted OEC is fully active in O_2 evolution despite the slower turnover rate, this suggests that the observed structural changes in the NO_3^--substituted OEC are also common to those in the native OEC.

In our previous study using the PS II membrane preparations, we inferred that an ionic NO_3^- is responsible for the isotopic bands, because the frequency region of the bands coincided with that of the NO asymmetric stretching modes of ionic NO_3^- (1440–1310 cm^{-1}) and the reported nitrato complexes with transient metals have no NO stretching modes in this frequency region (Gatehouse et al., 1958; Kato and Rolfe, 1967; Addison et al., 1971; Nakamoto, 1997; Waterland et al., 2001). However, it is essential to define the absence of isotopic bands at frequencies other than the region for the ionic NO_3^-, as the NO stretching modes of the NO_3^- bound to transient metals appear at 1635–1440 cm^{-1} and 1310–963 cm^{-1} (Gatehouse et al., 1958; Addison et al., 1971; Nakamoto, 1997). As shown in Fig. 4 *A*, the quality of the isotopic difference spectra was so high that we conclude that no isotopic band is induced in the 2140–1420 cm^{-1} and 1280–940 cm^{-1} regions in the spectra. We note in this context that an isotopic band may be canceled or very significantly reduced if a band shifted by the isotopic effect coincidently overlaps with another existing band with opposite sign. However, this possibility is less likely because the absence of the isotopic bands for the metal-bound form was evident in both isotopic spectra, in which the NO and NO_2 stretching modes of NO_3^- shift by 31 cm^{-1} (for $^{14}N/^{15}N$) and by 20 cm^{-1} (for $^{16}O/^{18}O$), respectively (Gatehouse et al., 1958). These considerations lead to the conclusion that only the ionic NO_3^- bands are induced in the S_2/S_1 FTIR difference spectrum. Therefore, the results provide evidence for the view that NO_3^- (or Cl^-) is bound to the Cl^- site coupling structurally with the Mn cluster presumably due to its location in close vicinity to the cluster, but NO_3^- (or Cl^-) is not associated with the cluster as a direct ligand.

Assignment of isotopic bands

The high quality isotopic difference spectra obtained in this study make it possible to assign the observed isotopic bands to the S_1 and S_2 states inductively. The assignment is crucial for the band analysis for understanding the role of NO_3^- (Cl^-) in the O_2 evolution. The isotopic difference spectra for the S_2/S_1 difference are formally expressed by the following equations:

$$^{14}N^{16}O_3^-/^{15}N^{16}O_3^- = {}^{14}N^{16}O_3^-[S_2] - {}^{14}N^{16}O_3^-[S_1] - {}^{15}N^{16}O_3^-[S_2] + {}^{15}N^{16}O_3^-[S_1] \quad (1)$$

$$^{14}N^{16}O_3^-/^{14}N^{18}O_3^- = {}^{14}N^{16}O_3^-[S_2] - {}^{14}N^{16}O_3^-[S_1] - {}^{14}N^{18}O_3^-[S_2] + {}^{14}N^{18}O_3^-[S_1], \quad (2)$$

where S_1 and S_2 in the brackets denote the S_1 state spectrum and the S_2 state spectrum, and the positive and negative signs imply that the corresponding spectra give positive and negative band(s) in the isotopic difference spectrum. Since $^{14}N^{16}O_3^-[S_2]$ and $^{14}N^{16}O_3^-[S_1]$ spectra equally contribute to both of the $^{14}N^{16}O_3^-/^{15}N^{16}O_3^-$ and $^{14}N^{16}O_3^-/^{14}N^{18}O_3^-$ difference spectra, the isotopic bands from these two spectra possibly appear identically in each isotopic difference spectrum if the putative bands do not overlap with other bands. Close inspection of the two isotopic difference spectra shown in Fig. 4 *B* revealed that band I appears at the same frequency at 1415 cm^{-1} with the same intensity and shape in each spectrum, but other bands do not show such coincidence. Therefore, band I is rationally assigned to the $^{14}N^{16}O_3^-$ mode in the S_1 state. According to Eqs. 1 and 2, possible candidates for the positive band II are the $^{14}N^{16}O_3^-[S_2]$ and $^{15}N^{16}O_3^-[S_1]$ spectra for the $^{14}N^{16}O_3^-/^{15}N^{16}O_3^-$ spectrum, and the $^{14}N^{16}O_3^-[S_2]$ and $^{14}N^{18}O_3^-[S_1]$ spectra for the $^{14}N^{16}O_3^-/^{14}N^{18}O_3^-$ spectrum, respectively. If the $^{15}N^{16}O_3^-[S_1]$ or $^{14}N^{18}O_3^-[S_1]$ spectrum is responsible for band II, a negative band due to the isotopic counterpart ($^{14}N^{16}O_3^-[S_1]$) must appear at the high frequency side of band II with intensity comparable to band II. This view, however, does not conform to the observed isotopic difference spectra at all. Therefore, it is concluded that the $^{14}N^{16}O_3^-$ mode of the S_2 spectrum should be ascribed to band II. The different manifestations of the same $^{14}N^{16}O_3^-[S_2]$ band between the two isotopic difference spectra are reasonably accounted for by the overlap of the positive band from the $^{15}N^{16}O_3^-[S_1]$ or $^{14}N^{18}O_3^-[S_1]$ spectrum, which is the isotopic counterpart of band I ($^{14}N^{16}O_3^-[S_1]$). The negative band III can be assigned to the $^{15}N^{16}O_3^-$ and $^{14}N^{18}O_3^-$ modes in the S_2 spectrum, which are the consequence of the downshift of band II ($^{14}N^{16}O_3^-[S_2]$) by the replacement of ^{14}N and ^{16}O by ^{15}N and ^{18}O, respectively. The possible candidates for the positive band IV are the $^{14}N^{16}O_3^-[S_2]$ and $^{15}N^{16}O_3^-[S_1]$ spectra for the $^{14}N^{16}O_3^-/^{15}N^{16}O_3^-$ spectrum, and the $^{14}N^{16}O_3^-[S_2]$ and $^{14}N^{18}O_3^-[S_1]$ spectra for the $^{14}N^{16}O_3^-/^{14}N^{18}O_3^-$ spectrum. If the $^{14}N^{16}O_3^-[S_2]$ spectrum is responsible for band IV, the negative band due to the isotopic counterpart ($^{15}N^{16}O_3^-[S_2]$ or $^{14}N^{18}O_3^-[S_2]$) must appear at the low frequency side of band IV, but such a band does not exist in the observed spectra. Therefore, it can be concluded that band IV should

be ascribed to the $^{15}N^{16}O_3^-$ and $^{14}N^{18}O_3^-$ modes in the S_1 spectrum for the $^{14}N^{16}O_3^-/^{15}N^{16}O_3^-$ and $^{14}N^{16}O_3^-/^{14}N^{18}O_3^-$ spectra, respectively. This assignment is reinforced by the fact that the frequency of band IV was higher by 10 cm^{-1} in the $^{14}N^{16}O_3^-/^{14}N^{18}O_3^-$ than in the $^{14}N^{16}O_3^-/^{15}N^{16}O_3^-$ spectrum, as expected.

Simulation of isotopic spectrum

The band assignments are summarized in Table 1 with the characteristic features of the respective bands. These clearly demonstrate that NO_3^- bound to the functional Cl^- site shows two bands at different frequencies in the S_1 state but only one band in the S_2 state. The observed $^{14}N^{16}O_3^-/^{15}N^{16}O_3^-$ difference spectrum was simulated by the use of information from these bands and by considering the isotopic band shifts. We note that the $^{14}N^{16}O_3^-/^{14}N^{18}O_3^-$ spectrum with the low ^{18}O enrichment is not applicable to a precise simulation study because the spectrum includes complex NO modes arising from NO_3^- with various $^{16}O/^{18}O$ combinations. Fig. 6 shows the result of simulation, in which the curve fitting for NO_3^- was carried out by a Lorentzian band shape that is frequently found in many nitrato complexes (Gatehouse et al., 1958; Kato and Rolfe, 1967; Addison et al., 1971; Nakamoto, 1997; Waterland et al., 2001). The overall features of the observed $^{14}N^{16}O_3^-/^{15}N^{16}O_3^-$ spectrum and fine structure, peak frequency, and intensity of each band were reproduced fairly well. The result demonstrates that the $^{14}N^{16}O_3^-$ bound to the Cl^- site reveals the two isolated sharp bands at 1415 and 1315 cm^{-1} in the S_1 state but one broad doublet band with adjacent peaks at 1370 and 1358 cm^{-1} in the S_2 state.

Interaction of NO_3^- (Cl^-) with the Cl^- site

The results of the band assignment and simulation can be interpreted in two alternative ways. The first interpretation is that a single NO_3^- ion bound to the Cl^- site produces two split bands in the S_1 state due to the geometrical asymmetry which has been often observed in salt crystals (Gatehouse et al., 1958; Addison et al., 1971; Nakamoto, 1997). The vibrational modes of the NO_3^- ion become to be generated to show one broad band with two adjacent peaks due to the more symmetric geometry of NO_3^- in the S_2 state. The second interpretation is that the two bands arise from NO_3^- ions bound to two different Cl^- sites. In the S_2 state, each of the two bands shifts in opposite directions to form a composite broad band. In this case, the geometry of the NO_3^- ion bound to each Cl^- site must be highly symmetric in the S_1 and S_2 states as revealed by the sharp single band. However, observed band positions in the S_1 state (1415 and 1315 cm^{-1}) deviate far from any frequencies of the symmetric NO_3^- (1385–1370 cm^{-1}) (Kato and Rolfe, 1967; Waterland et al., 2001). We therefore exclude this possibility and conclude that the isotopic bands arise from the NO_3^- ion bound to a unique Cl^- site in the OEC, in which the geometry of the NO_3^- ion is highly asymmetric in the S_1 state and very symmetrical in the S_2 state. Although how the geometry change of the NO_3^- ion is achieved has not been resolved, a good possibility is that NO_3^- strongly interacts with a positively charged amino acid residue in the S_1 state to be largely constrained, but the interaction weakens and the geometry becomes symmetrical in the S_2 state.

The apparent *K*m value of NO_3^- for the isotopic band was deduced on the basis of the intensity of band II plus band III, which are assigned to the S_2 state. Therefore, the obtained *K*m represents the value in the S_2 state. It is of note in this context that the intensity of band IV shows roughly the same NO_3^- concentration dependence as that of band II and band III as shown in Fig. 5 *A*, although the smaller band intensity may not allow us to determine *K*m reliably. As the $^{15}N^{16}O_3^-$ modes in the S_1 state are exclusively responsible for this band, the results indicate that the *K*m value of NO_3^- in the S_1 state resembles that in the S_2 state. Furthermore, taking into account the apparent *K*m for O_2 evolution, the *K*m of NO_3^- in every S state may not be higher than the value of ~6 mM. These observations suggest that affinities of NO_3^- to the Cl^- site do not differ much among all the S states. It is therefore likely that the much higher NO_3^- substitution rate in the S_2

TABLE 1 Vibrational assignments of $^{14}N^{16}O_3^-/^{15}N^{16}O_3^-$ and $^{14}N^{16}O_3^-/^{14}N^{18}O_3^-$ isotopic bands

Spectrum*	Band (sign)	Position (cm^{-1})	Intensity		Assignments
			$\Delta A \times 10^{-5}$	(area, rel., %)	
$^{14}N^{16}O_3^-$ (S_2/S_1)/$^{15}N^{16}O_3^-$ (S_2/S_1)	I(−)†	1415	2.0	30	$^{14}N^{16}O_3^-$ [S_1]
	II(+)	1369	6.7	100	$^{14}N^{16}O_3^-$ [S_2], ($^{15}N^{16}O_3^-$ [S_1])‡
	III(−)	1319	5.3	79	$^{15}N^{16}O_3^-$ [S_2], ($^{14}N^{16}O_3^-$ [S_1])
	IV(+)	1284	3.4	51	$^{15}N^{16}O_3^-$ [S_1]
$^{14}N^{16}O_3^-$ (S_2/S_1)/$^{14}N^{18}O_3^-$ (S_2/S_1)	I(−)	1415	1.9	37	$^{14}N^{16}O_3^-$ [S_1]
	II(+)	1377	5.1	100	$^{14}N^{16}O_3^-$ [S_2], ($^{14}N^{18}O_3^-$ [S_1])
	III(−)	1321	5.0	98	$^{14}N^{18}O_3^-$ [S_2], ($^{14}N^{16}O_3^-$ [S_1])
	IV(+)	1294	2.2	43	$^{14}N^{18}O_3^-$ [S_1]

*40 mM $NaNO_3$ was added in the Cl^- depleted PS II core particles.
†Plus and minus signs represent positive and negative bands, respectively.
‡Minor contribution.

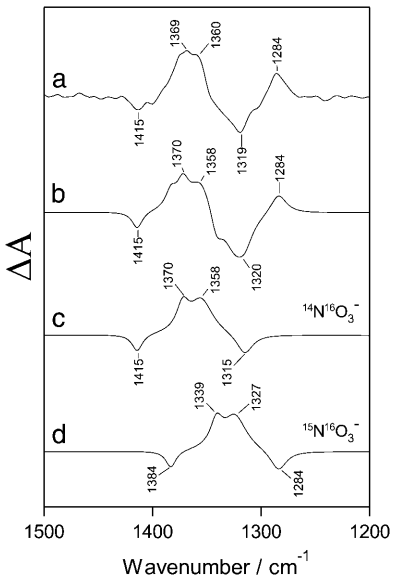

FIGURE 6 Simulation of the $^{14}N^{16}O_3^-/^{15}N^{16}O_3^-$ isotopic bands for the S_2/S_1 difference. Experimentally obtained (*a*) and simulated (*b*) $^{14}N^{16}O_3^-/^{15}N^{16}O_3^-$ spectrum (*a*) for $S_2Q_A^-/S_1Q_A$ difference, and simulated $^{14}N^{16}O_3^-$ (*c*) and simulated $^{15}N^{16}O_3^-$ (*d*) spectra for the S_2/S_1 difference. The difference spectrum for the $S_2Q_A^-/S_1Q_A$ difference is identical to that for the S_2/S_1 difference but has a better signal/noise ratio.

than the S_1 state (Wincencjusz et al., 1998) is caused by the lowered Cl^- affinity and/or the facilitation of the replacement of Cl^- by NO_3^- due to the more symmetric geometry for Cl^- in the S_2 state.

Several types of Cl^--binding sites have been reported in the PS II membranes which were washed with and dialyzed against Cl^--free medium (Lindberg et al., 1993; Lindberg and Andréasson, 1996; Olesen and Andréasson, 2003). Some of them have higher affinity for Cl^- as compared with the site observed in this study, or show affinity to NO_3^- (Lindberg et al., 1993). The higher Cl^- affinity in the dialyzed membranes may be mainly ascribed to the presence of the 16- and 24-kDa proteins, which are completely removed in the core particles used in this study. However, we should emphasize in this context that most OECs in the dialyzed membranes have been reported to be active in O_2 evolution when measured at light-limiting conditions (Lindberg et al., 1993; Lindberg and Andréasson, 1996; Olesen and Andréasson, 2003), but the Cl^--depleted PS II core particles used in this study and the Cl^--depleted PS II membranes (Hasegawa et al., 2002) have shown eventually no O_2 evolution even at the light-limiting conditions. Therefore, the functional Cl^- site analyzed by FTIR in this study may be different from the nonfunctional sites detected in the dialyzed membranes.

The isotopic FTIR study makes it possible to monitor directly the NO_3^- ion functionally bound to the Cl^- site in the OEC and its structural change upon the oxidation of the Mn cluster to the S_2 state. Since NO_3^- is functional for supporting O_2 evolution, most of the knowledge obtained may be directly applicable to Cl^-.

In general, nitrate is a planar molecule coordinated by three ligands, whereas chloride is a spherical molecule coordinated with three to six ligands. The functional binding of NO_3^- to the Cl^- site suggests that coordination geometry of Cl^- in the binding site is rather similar to that of NO_3^- in the OEC. In fact, both NO_3^- and Cl^- are functionally bound to the allosteric site of subunit type II hemocyanin, in which Cl^- is coordinated in trigonal planar-like geometry by the same three protein ligands as NO_3^- (Hazes et al., 1993, 1996; Bart et al., 1996). Similarly, Cl^- in the active center of halorhodopsin accepts only three hydrogen bonds (Kolbe et al., 2002), and NO_3^- is able to bind to the site (Sato et al., 2002). Cl^- is involved in the ionic interactions with three amino acid residues and two water molecules as an analog of a trigonal planar sulfide ion in an allosteric site of *O*-acetylserine sulfhydrylase (Burkhard et al., 2002). Therefore, we may propose that Cl^- associates with a limited number of amino acid residues and water molecules in quasi-trigonal planar geometry at the Cl^- site in the OEC.

This work was supported by grants for the Frontier Research System at RIKEN and Grant-in-Aid for Scientific Research (13640695) (to T.O.) from Ministry of Education, Culture, Sports, Science and Technology of Japan.

REFERENCES

Addison, C. C., N. Logan, S. C. Wallwork, and C. D. Garner. 1971. Structural aspects of coordinated nitrate groups. *Q. Rev. Chem. Soc.* 25:289–322.

Akabori, K., A. Imaoka, and Y. Toyoshima. 1984. The role of lipid and 17-kDa protein in enhancing the recovery of O_2 evolution in cholate-treated thylakoid membranes. *FEBS Lett.* 173:36–40.

Bart, H., K. A. Magnus, K. H. Kalk, C. Bonaventura, and W. G. J. Hol. 1996. Nitrate binding to *Limulus polyphemus* subunit type II hemocyanin and its functional implications. *J. Mol. Biol.* 262:532–542.

Berthold, D. A., G. T. Babcock, and C. F. Yocum. 1981. A highly resolved, oxygen-evolving photosystem II preparation from spinach thylakoid membranes. *FEBS Lett.* 134:231–234.

Berthomieu, C., E. Nabedryk, W. Mäntele, and J. Breton. 1990. Characterization by FTIR spectroscopy of photoreduction of the primary quinone acceptor Q_A in photosystem II. *FEBS Lett.* 269:363–367.

Boussac, A. 1995. Exchange of chloride by bromide in the manganese photosystem-II complex studied by cw- and pulsed-EPR. *Chem. Phys.* 194:409–418.

Burkhard, P., C. H. Tai, J. N. Jansorivs, and P. F. Cook. 2002. Identification of an allosteric anion-binding site on *O*-acetylserine sulfhydrylase: structure of the enzyme with chloride bound. *J. Mol. Biol.* 303: 279–286.

Casey, J. L., and K. Sauer. 1984. EPR detection of a cryogenically photogenerated intermediate in photosynthetic oxygen evolution. *Biochim. Biophys. Acta.* 767:21–28.

Crichley, C. 1985. The role of chloride in photosystem II. *Biochim. Biophys. Acta.* 811:33–46.

Debus, R. J. 1992. The manganese and calcium ions of photosynthetic oxygen evolution. *Biochim. Biophys. Acta.* 1102:269–352.

Gatehouse, B. M., S. E. Livingstone, and R. S. Nyholm. 1958. Infrared spectra of some nitrato and other oxyanion coordination complexes. *J. Inorg. Nucl. Chem.* 8:75–78.

Goussias, C., A. Boussac, and A. W. Rutherford. 2002. Photosystem II and photosynthetic oxidation of water: an overview. *Philos. Trans. R. Soc. Lond. B Biol. Sci.* 357:1369–1381.

Hasegawa, K., Y. Kimura, and T. Ono. 2002. Chloride cofactor in the photosynthetic oxygen-evolving complex studied by Fourier transform infrared spectroscopy. *Biochemistry.* 41:13839–13850.

Hazes, B., K. A. Magnus, C. Bonaventura, J. Bonaventura, Z. Dauter, K. H. Kalk, and W. G. J. Hol. 1993. Crystal structure of deoxygenated *Limulus polyphemus* subunit II hemocyanin at 2.18 Å resolution: clues for a mechanism for allosteric regulation. *Protein Sci.* 2:597–619.

Hazes, B., K. A. Magnus, K. H. Kalk, C. Bonaventura, and W. G. J. Hol. 1996. Nitrate binding to *Limulus polyphemus* subunit type II hemocyanin and its functional implications. *J. Mol. Biol.* 262:532–542.

Hienerwadel, R., A. Boussac, J. Breton, and C. Berthomieu. 1996. Fourier transform infrared difference study to $Tyrosine_D$ oxidation and plastoquinone Q_A reduction in photosystem II. *Biochemistry.* 35:15447–15460.

Homann, P. H. 1987. The relation between the chloride, calcium, and polypeptide requirements of photosynthetic water oxidation. *J. Bioenerg. Biomembr.* 19:105–123.

Homann, P. H. 1988. Chloride relations of photosystem II membrane preparations depleted of, and resupplied with, their 17 and 23 kDa extrinsic polypeptides. *Photosynth. Res.* 15:205–220.

Homann, P. H. 2002. Chloride and calcium in photosystem II: from effects to enigma. *Photosynth. Res.* 73:169–175.

Homann, P. H., H. Gleiter, T. Ono, and Y. Inoue. 1986. Storage of abnormal oxidants '$\sum_1$', '$\sum_2$' and '$\sum_3$' in photosynthetic water oxidases inhibited by Cl^- removal. Biochim. Biophys. Acta. 850:10–20.

Itoh, S., C. T. Yerkes, H. Koike, H. H. Robimson, and A. R. Crofts. 1984. Effects of chloride depletion on electron donation from the water-oxidizing complex to the photosystem II reaction center as measured by the microsecond rise of chlorophyll fluorescence in isolated pea chloroplasts. *Biochim. Biophys. Acta.* 766:612–622.

Kato, R., and J. Rolfe. 1967. Vibration frequencies of NO_2^- and NO_3^- ions in KBr crystals. *J. Chem. Phys.* 47:1901–1910.

Kimura, Y., K. Hasegawa, and T. Ono. 2002. Characteristic changes of the S_2/S_1 difference FTIR spectrum induced by Ca^{2+}-depletion and metal cation substitution in photosynthetic oxygen-evolving complex. *Biochemistry.* 41:5844–5853.

Kimura, Y., and T. Ono. 2001. Chelator-induced disappearance of carboxylate stretching vibrational modes in S_2/S_1 FTIR spectrum in oxygen-evolving complex of photosystem II. *Biochemistry.* 40:14061–14068.

Klein, M. P., K. Sauer, and V. K. Yachandra. 1993. Perspectives on the structure of the photosynthetic oxygen evolving manganese complex and its relation to the Kok cycle. *Photosynth. Res.* 38:265–277.

Kolbe, M., H. Besir, L. O. Essen, and D. Oesterhelt. 2002. Structure of the light-driven chloride pump halorhodopsin at 1.8 Å resolution. *Science.* 288:1390–1396.

Lindberg, K., and L. E. Andréasson. 1996. A one-site, two-site model for the binding of anions in photosystem II. *Biochemistry.* 35:14259–14267.

Lindberg, K., T. Vängård, and L. E. Andréasson. 1993. Studies of the slowly exchanging chloride in photosystem II of higher plants. *Photosynth. Res.* 38:401–408.

Lindberg, K., T. Wydrzynski, T. Vänngård, and L.-E. Andréasson. 1990. Slow release of chloride from ^{36}Cl-labeled photosystem II membranes. *FEBS Lett.* 264:153–155.

Miyao, M., and N. Murata. 1985. The Cl^- effect on photosynthetic oxygen evolution: interaction of Cl^- with 18-kDa, 24-kDa and 33-kDa proteins. *FEBS Lett.* 180:303–308.

Nakamoto, K. 1997. Infrared and Raman Spectra of Inorganic and Coordination Compounds. Part B: Application in Coordination, Organometallic, and Bioinorganic Chemistry, 5th ed. John Wiley & Sons Inc., New York.

Noguchi, T., T. Ono, and Y. Inoue. 1992. Detection of structural changes upon S_1-to-S_2 transition in the oxygen-evolving manganese cluster in photosystem II by light-induced Fourier transform infrared difference spectroscopy. *Biochemistry.* 31:5953–5956.

Noguchi, T., T. Ono, and Y. Inoue. 1995a. Direct detection of a carboxylate bridge between Mn and Ca^{2+} in the photosynthetic oxygen-evolving center by means of Fourier transform infrared spectroscopy. *Biochim. Biophys. Acta.* 1228:189–200.

Noguchi, T., T. Ono, and Y. Inoue. 1995b. A carboxylate ligand interacting with water in the oxygen-evolving center of photosystem II as revealed by Fourier transform infrared spectroscopy. *Biochim. Biophys. Acta.* 1232:59–66.

Noguchi, T., and M. Sugiura. 2003. Analysis of flash-induced FTIR difference spectra of the S-state cycle in the photosynthetic water-oxidizing complex by uniform ^{15}N and ^{13}C isotope labeling. *Biochemistry.* 42:6035–6042.

Olesen, K., and L. E. Andréasson. 2003. The function of the chloride ion in photosynthetic oxygen evolution. *Biochemistry.* 42:2025–2035.

Ono, T., and Y. Inoue. 1985. S-state turnover in the O_2-evolving system of $CaCl_2$-washed photosystem II particles depleted of three peripheral proteins as measured by thermoluminescence: removal of 33 kDa protein inhibits S_3 to S_4 transition. *Biochim. Biophys. Acta.* 806:331–340.

Ono, T., T. Noguchi, Y. Inoue, M. Kusunoki, H. Yamaguchi, and H. Oyanagi. 1995. XANES spectroscopy for monitoring intermediate reaction states of Cl^--depleted Mn cluster in photosynthetic water oxidation enzyme. *J. Am. Chem. Soc.* 117:6386–6387.

Ono, T., J. L. Zimmermann, Y. Inoue, and A. W. Rutherford. 1986. EPR evidence for a modified S-state transition in chloride-depleted photosystem II. *Biochim. Biophys. Acta.* 851:193–201.

Onoda, K., H. Mino, Y. Inoue, and T. Noguchi. 2000. An FTIR study on the structure of the oxygen-evolving Mn-cluster of photosystem II in different spin forms of the S_2-state. *Photosynth. Res.* 63:47–57.

Razeghifard, M. R., S. Kim, J. S. Patzlaff, R. S. Hutchison, T. Krick, I. Ayala, J. J. Steenhuis, S. E. Boesch, R. A. Wheeler, and B. A. Barry. 1999. In vivo, in vitro, and calculated vibrational spectra of plastoquinone and the plastosemiquinone anion radical. *J. Phys. Chem. B.* 103:9790–9800.

Sato, M., T. Kanamori, N. Kamo, M. Demura, and K. Nitta. 2002. Stopped-flow analysis on anion binding to blue-form halorhodopsin from *Natronobacterium pharaonis*: comparison with the anion-uptake process during the photocycle. *Biochemistry.* 41:2452–2458.

Sinclair, J. 1994. Changes in thylakoid behaviour in chloride-free media. *Biochim. Biophys. Acta.* 1185:112–118.

Theg, S. M., P. A. Jursinic, and P. H. Homann. 1984. Studies on the mechanism of chloride action on photosynthetic water oxidation. *Biochim. Biophys. Acta.* 766:636–646.

Waterland, M. R., D. Stockwell, and A. M. Kelley. 2001. Symmetry breaking effects in NO_3^-: Raman spectra of nitrate salts and ab initio resonance Raman spectra of nitrate-water complexes. *J. Chem. Phys.* 114:6249–6258.

Wincencjusz, H., H. J. van Gorkom, and C. F. Yocum. 1997. The photosynthetic oxygen evolving complex requires chloride for its redox state $S_2 \rightarrow S_3$ and $S_3 \rightarrow S_0$ transitions but not for $S_0 \rightarrow S_1$ or $S_1 \rightarrow S_2$ transitions. *Biochemistry.* 36:3663–3670.

Wincencjusz, H., C. F. Yocum, and H. J. van Gorkom. 1998. S-state dependence of chloride binding affinities and exchange dynamics in the intact and polypeptide-depleted O_2 evolving complex of photosystem II. *Biochemistry.* 37:8595–8604.

Wincencjusz, H., C. F. Yocum, and H. J. van Gorkom. 1999. Activating anions that replace Cl^- in the O_2-evolving complex of photosystem II slow the kinetics of the terminal step in water oxidation and destabilize the S_2 and S_3 states. *Biochemistry.* 38:3719–3725.